Determination of strain localization in aluminum alloys using laser-induced photoelectron emission

M. Cai and S. C. Langford
Physics Department, Washington State University, Pullman, Washington 99164-2814

L. E. Levine
National Institute of Standards and Technology, 100 Bureau Dr., Gaithersburg, Maryland 20899-8553

J. T. Dickinson[a)]
Physics Department, Washington State University, Pullman, Washington 99164-2814

(Received 27 July 2004; accepted 21 September 2004)

Uniaxial tensile deformation of oxidized aluminum produces low work-function patches of fresh metal which can be probed by measurements of photoelectron emission during exposure to ultraviolet light. We report measurements of photoelectron emission during uniaxial testing of polycrystalline Al(1200), Al–Mn(3003), Al–Mg(5052), and Al–Mg–Si(6061) alloys where the broad face of the gauge section is exposed to pulsed excimer laser radiation (248 nm). We show that strain localization alters the distribution of fresh surface metal produced by subsequent deformation. The transition from more homogenous deformation to the principally localized deformation associated with shear bands is associated with a discontinuity in the growth rate of photoelectron intensities versus time. At this transition, the rate of fresh metal production along the illuminated portion of gauge section decreases. In all four materials, the strain at the discontinuity is somewhat below the strain given by the Considère criterion, consistent with the role of microstructural effects in strain localization. We suggest that these photoelectron measurements constrain quantitative models of strain localization. © *2004 American Institute of Physics*. [DOI: 10.1063/1.1814420]

I. INTRODUCTION

The deformation of metal structures is strongly affected by strain localization (or instability). Considère,[1] Hart,[2] Hillier,[3] and Duncombe[4,5] have provided important descriptions of strain localization. Nichols[6] developed a sophisticated criterion for the onset of tensile instability based on a long-wavelength uniaxial stress approximation. Tensile deformation is complicated by the complex evolution of microstructure and geometry. Microstructure changes include solute diffusion (responsible for the Portevin-Le Châtelier effect)[7] and dislocation interactions. Strain rate also influences the deformation behaviors; those effects include thermal softening and strain hardening.[6,8–14]

Few experiments are capable of testing models of strain localization in a fundamental fashion. Measurements of maximum stress capacity assess sample stability during tensile or creep tests, but are susceptible to changes in internal microstructural accompanying strain hardening.[6,8–14] High-speed photography has been employed to monitor strain localization in pure shear loading,[15] but data analysis to date is largely empirical.

In this work, we report measurements of UV laser-stimulated electron emission from polycrystalline aluminum during uniaxial tensile deformation. These signals show distinctive changes at strains consistent with the onset of strain localization. These observed changes are somewhat below the onset predicted by the Considère criterion. This is consistent with current models of strain localization, which predict localization at lower strains due to microstructural effects. Strain localization occurs at relatively large strains and is characterized by the formation of macroscopic shear bands.[16] The transition to strain localization can be monitored by photostimulated electron (PSE) emission because the rate of new surface area production per unit strain is different before and after localization.

It is important to stress that the increase in the PSE signal during deformation is proportional to the area of fresh metal surface exposed as slip lines and bands intersect the surface,[17] with possibly minor effects due to grain rotation. The tendency of the native oxide on aluminum to hinder PSE allows for sensitive measurements of the formation of new surface area. Earlier work showed that deformation of aluminum (and other metals such as titanium and magnesium) greatly increased the emission of electrons by chemisorption of oxygen.[18] This emission unambiguously requires the exposure of fresh metal. This increase in area is expected to increase the photoemission intensities under 248-nm illumination and is the likely source of the intensity increases described below.

II. EXPERIMENT

Four aluminum alloys, 1200, 3003, 5052, and 6061, were received in a rolled sheet with a thickness of 0.80 mm. The nominal chemical compositions of the alloys are shown in Table I. The alloy sheets were machined into dog-bone tensile specimens (parallel to the rolling direction) with a gauge length of 25.4 mm and width of 4 mm. Tensile speci-

[a)]Author to whom correspondence should be addressed; Electronic mail: jtd@wsu.edu

TABLE I. Chemical composition of the alloys (wt %) used in this work.

Alloy	Si	Cu	Mn	Mg	Fe
1200	$<1.0^a$				
3003	0.6		1.0–1.5		0.7
5052	0.25	0.10	0.10	2.2–2.8	
6061	0.73	0.35	0.002	0.85	0.17

[a]wt %Fe+wt %Si$\leq$1.0.

mens were paste polished, ultrasonically cleaned with acetone, and annealed in air for 3 h at 300 °C to produce an oxide layer ~4 nm thick. The polycrystalline samples were mounted in a vacuum compatible tensile testing apparatus. Testing was carried out at a constant crosshead speed of 0.032 mm/s to yield nominal strain rates of 1.25×10^{-3} s^{-1} at the onset of testing and 0.9×10^{-3} s^{-1} at a strain of 0.40.

Photoemission experiments were performed in a stainless-steel vacuum system at pressures of about 1×10^{-6} Pa. Figure 1 shows a schematic of the apparatus. The total pressure was monitored by a Bayard-Alpert ionization gauge. Electron emission was detected with a Burle Electro-optics Model 4716 Channeltron electron multiplier (CEM) operated at a gain of approximately 10^6 mounted 150 mm from the sample. The CEM output was amplified with fast electronics (time constant for rise/decay typically 10 ns) and digitized by a digital oscilloscope. Electron emission due to each laser pulse was digitized individually for a total of 250 laser pulses during a typical tensile deformation cycle.

The oxide thickness was determined by x-ray photoelectron spectroscopy (XPS). Spectra were acquired with a Kratos Axis 165 photoelectron spectrometer using a dual Mg Kα source and a Vision control and data system. The hemispherical electron energy analyzer was operated in the electrostatic magnification, fixed analyzer transmission mode. Kinetic energies were measured at increments of 0.1 eV with a pass energy of 40 eV. Oxide thickness was determined by taking the ratio of the intensities of primary, zero-loss photoelectron peaks corresponding to the oxide and the metal.[19–23]

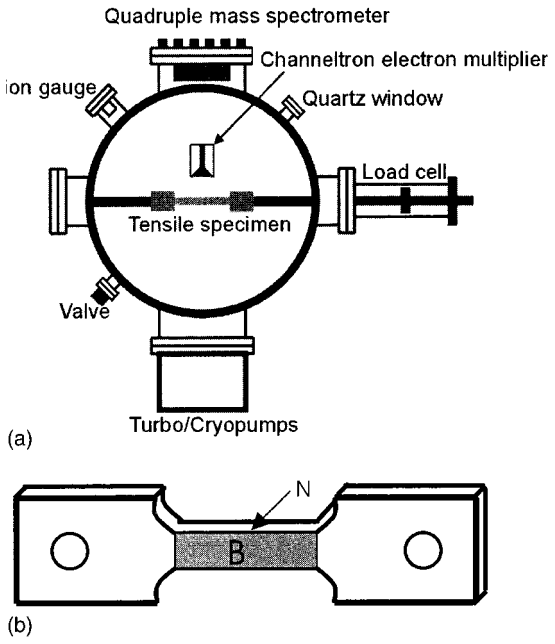

FIG. 1. (a) Schematic of apparatus to detect photostimulated electron emission during tensile testing. (b) A diagram of the configuration of the tensile specimens. The broad surface of the gauge section is shaded and labeled B and was illuminated by laser. The narrow surface of the gauge section, labeled N, was not illuminated by laser.

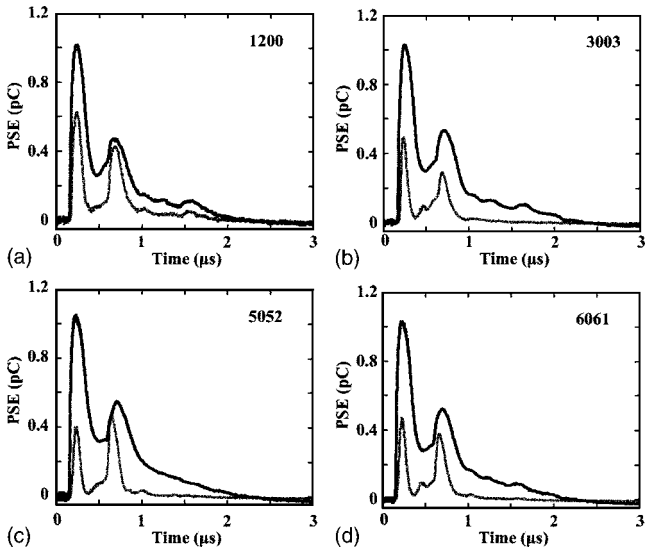

FIG. 2. Photostimulated electron (PSE) signals vs time due to single laser pulses before (gray dots) and after (black dots) deformation of (a) 1200, (b) 3003, (c) 5052, and (d) 6061 aluminum alloys. The laser pulse was incident on the samples at the time $t=0$ on the horizontal scale.

Pulsed laser radiation at 248-nm was provided by a Lambda Physik Lextra 200 excimer laser (KrF, 30-ns pulses) operated at a repetition rate of 2 Hz. The wavelength used for a given surface is important; we attempt to minimize the emission before any deformation while maximizing emission rates from the freshly exposed surfaces. The laser output was attenuated with interference filters to achieve a total fluence of about 500 $\mu J/cm^2$ at the sample. The laser radiation was incident on the broad surface of the sample gauge section, which is shaded and labeled B in Fig. 1.

III. RESULTS

A. Electron time-of-flight signals

Typical PSE signals accompanying single laser pulses before and after significant elongation (i.e., immediately before and after failure) of the four alloys appear in Fig. 2. The laser pulse was delivered to the sample at the time $t=0$ μs. All signals show peaks at about 0.24 and 0.64 μs after the laser pulse; as we show below, these arrival times are consistent with low-energy electrons moving between sample and detector. The intensity of the first peak, denoted peak I, is a strong function of strain in each of the four alloys and displays a weak tail that continues for 2–3 μs. The second peak, peak II, overlaps the tail of peak I. When the tail is subtracted from the signal, peak II is a very weak function of strain.

The intensities of both peaks I and II are strong functions of oxide thickness. Figure 3(a) shows XPS spectra of three aluminum samples with oxides produced by three different

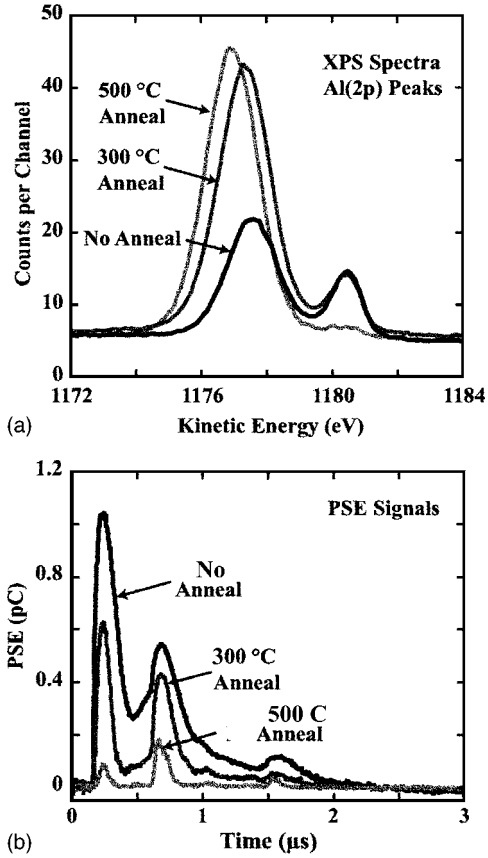

FIG. 3. (a) XPS spectra of 1200 aluminum, used to determine the oxide thicknesses. The low kinetic energy peak cirresponds to emission from the Al(2*p*) state of the oxide, and the high kinetic energy peak is due to emission from the Al(2*p*) state of the metal. One sample was mounted in vacuum immediately after polishing and cleaning (no anneal) and displayed an oxide thickness of 28 Å. A second sample was annealed for 3 h in air at 300 °C and displayed an oxide thickness of 42 Å. A third sample was annealed in air for 10 h at 500 °C and displayed an oxide thickness of 62 Å. (b) PSE signals from the three samples with different oxide thicknesses.

treatments. One sample was loaded into the vacuum system immediately after polishing and cleaning (no anneal); the corresponding XPS signal is consistent with an oxide thickness of 28 Å. A second sample was annealed at 300 °C in air for 3 h, and displays a 42-Å oxide. A third sample was annealed in air at 500 °C for 10 h to produce a thicker, 62 Å oxide.

Figure 3(b) shows the corresponding PSE signals from these three samples. The PSE from the as-polished (not annealed) sample shows intense peak I and peak II signals. The 300 °C anneal reduced the intensity of peak I by half and actually increased the intensity of peak II. The longest anneal (at 500 °C reduced the intensities of both peaks I and II to low values. The peak showing the most sensitivity to the presence of the oxide is peak I.

We propose the following interpretation of the two peaks. Peak I is associated with shorter time of flights (higher kinetic energies) and reduced intensities in the presence of thicker oxides, suggesting that the electrons that form peak I interact only weakly with the oxide layer, if any. Electrons emitted from fresh aluminum surfaces produced by deformation likely appear in peak I. In the presence of an oxide, electrons passing through the oxide layer with minimal scattering would also appear in peak I. In contrast, peak II appears to consist of electrons which have undergone inelastic scattering events within the oxide layer. The presence of two peaks on the underformed surface is due to the patchy nature of thermal oxides on aluminum.[24–26] Photoelectrons are more likely to penetrate thin portions of the 28- and 42-Å oxides without scattering. The highest amplitude peak I signal for the 28-Å oxide is consistent with larger portions of thin oxide on that sample. As the oxide thickness increases, the fraction of scattered electrons increases, accounting for the fairly robust peak II signal from the sample with the 42-Å oxide; nevertheless, attenuation of both peaks results in an overall drop in the number of transmitted electrons relative to the sample with the 28-Å oxide. For sufficiently thick oxides, e.g., 62 Å, even peak II is strongly attenuated. In addition to scattering photoelectrons, the oxide is expected to provide a roughly 2-eV barrier to photoelectron tunneling;[25] thus the thicker the oxide, the lower the electron intensity [Fig. 3(b)].

We have modeled the electric fields of the experimental arrangement inside our vacuum system using finite difference solutions to Laplace's equation.[27] This allows us to determine predicted electron trajectories and time of flights for various initial kinetic energies and launch angles relative to the surface normal. The peak time of flight in peak I corresponds to an average kinetic energy of approximately 0.7 eV. Although the work functions of oxidized, alloy surfaces are not well defined, an electron kinetic energy of 0.7 eV is reasonably consistent with emission from polycrystalline aluminum (work function 4.28 eV) exposed to 248-nm (5.0 eV) photons. Numerical calculations predict a kinetic energy of <0.1 eV for peak II, consistent with significant energy loss due to inelastic scattering in the oxide layer.

As previously noted, the PSE observed prior to deformation constitutes an unwanted background. Although these signals can be minimized by oxidizing treatments, very thick oxide reduces the sensitivity of peak I to deformation. Reasonably good results were obtained by annealing treatments that produced an average oxide thickness of 40 Å.

B. PSE versus strain

We first show how the total electron emission changes as samples of each alloy are elongated. The total charge delivered by the electron detector for each laser pulse was determined by integrating the PSE signal from 0 to 2.2 μs. This total integrated charge is plotted versus strain in Fig. 4. For comparison purposes, the nominal stress-strain curve for each experiment is also shown. In general, the PSE intensities increase gradually during the initial stages of loading. As the strain reaches about 0.04, the intensities increase more rapidly.

Because peak I is especially sensitive to changes in surface topography, i.e., new surface area produced on the broad surface of the gauge length, we concentrate on peak I only. A plot of peak I intensities versus strain for all four sample types appear in Fig. 5. In each case, two linear regions of PSE growth can be identified, with a transition located at

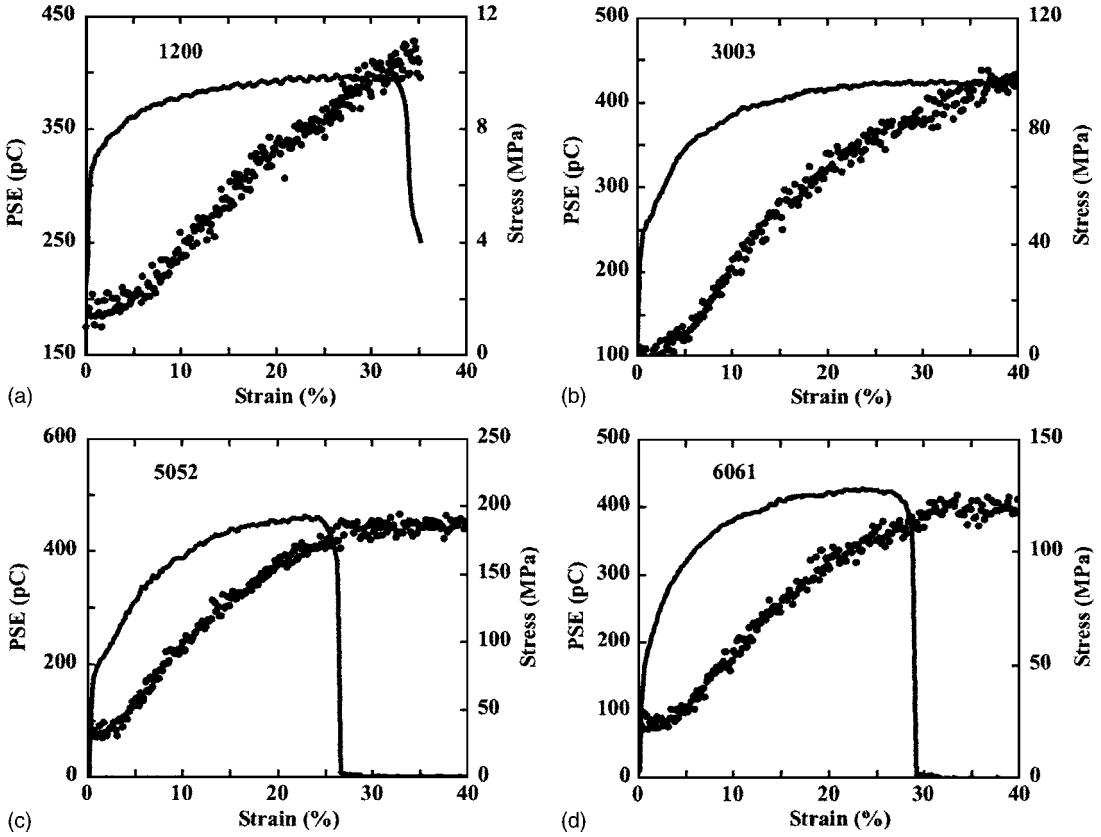

FIG. 4. Integrated (total) PSE signals and nominal stress as functions of strain during tensile testing of (a) 1200, (b) 3003, (c) 5052, and (d) 6061 aluminum alloys.

nominal strains between 0.15 and 0.20. We identify the transition between these two linear regions with the onset of strain localization.

Interestingly, we consistently observe that the pulse-to-pulse fluctuations in the PSE intensities increase significantly after the discontinuity in slope, i.e., after the onset of strain localization. Although further study is required to determine the source of these fluctuations, we note that the relatively easy slip along shear bands after localization can locally relax or enhance plastic strains in nearby grains, depending on their strain history and orientation relative to the band. This would account for fluctuations in PSE intensity as shear bands propagate along the gauge section.

C. Considère criterion

Although strain localization is a complex phenomenon involving both microstructural and mechanical effects, the strain at the onset of localization is bounded from above by the geometrical, mechanical instability described by the Considère criterion.[1] The Considère criterion has the advantage of being directly determined from stress-strain data. The criterion itself is given by

$$\frac{d\sigma_t}{d\varepsilon_t} = \sigma_t, \tag{1}$$

where σ_t and ε_t are the true stress and strain, respectively.

Table II lists the strain value at which the Considère criterion is satisfied for the four tested alloys in this work, along with the strain value marking the transition between the two linear regions of PSE growth determined from the slopes in Fig. 5. In each case, the Considère strain is somewhat higher than the onset of strain localization as determined from the PSE measurements—consistent with the upper bound on strain localization provided by the criterion.

IV. DISCUSSION

The photostimulated emission of electrons during tensile deformation and fracture was reported in the 1950s and a number of interesting studies followed.[17,18,28–40] Electron microscopy, autoradiographic stripping,[29] and photoemission spectroscopy[17,37] showed that these signals were closely associated with the formation of slip lines and bands on deformed surfaces. Baxter and co-workers exploited the sensitivity of PSE to microstructural changes in several studies of fatigue and deformation.[17,33–37,41] They reported a linear increase of PSE with tensile strain during the deformation of copper and aluminum over a strain range from 0 to about 0.10—consistent with the linear increase observed in this work prior to localization. This range of strains excludes the onset of strain localization,[33,35] which was not probed.

Deformation of aluminum alloys is largely confined to slip on well-defined planes. In polycrystals tested at a constant strain rate, deformation occurs first in grains with preferred orientations. As strain increases, grain rotation and stress concentration eventually produce an assembly of grains that deforms more uniformly (Taylor model).[42,43] Sub-

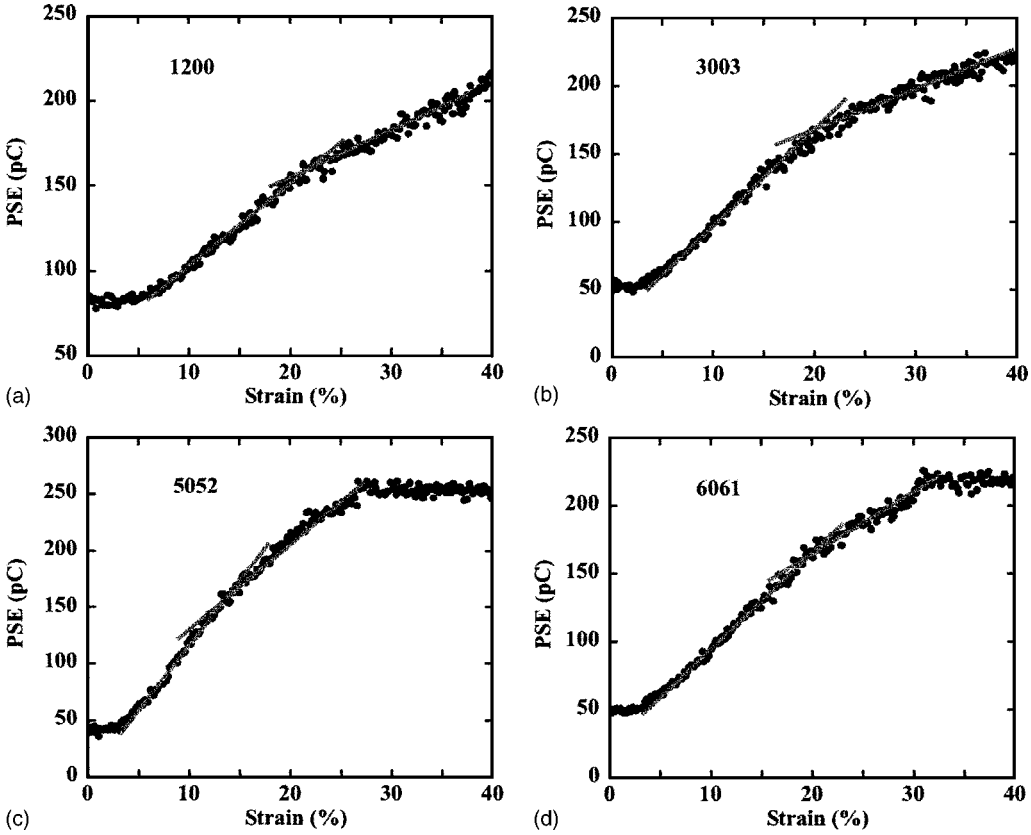

FIG. 5. Integrated PSE signals corresponding to peak I (fast electrons) vs strain during tensile testing of (a) 1200, (b) 3003, (c) 5052, and (d) 6061 aluminum alloys.

sequent strain is accommodated by the stable production of slip lines and bands within all grains. At a constant crosshead speed, the increase in sample area per unit time due to the production of fresh metal surface during stable deformation is expected to be constant and relatively uniform along the surfaces of the gauge section. Both the broad surface, labeled B in Fig. 1 and illuminated by laser, and the narrow surface, labeled N in Fig. 1 and not illuminated by the laser, are deformed uniformly. This accounts for the first linear part of PSE versus strain curve.

As deformation proceeds, this relatively homogenous deformation is disrupted by localized slip on shear bands that extend across the sample. Subsequent dislocation motion is largely confined to these bands. Although the detailed thermodynamics and kinetics of strain localization are beyond the scope of this paper, the competition between localization and work hardening effects soon yields a second stable deformation period that operates until failure. Dislocations propagating along these shear bands intersect the narrow surface of the gauge section, labeled N, where they produce increasing amounts of fresh metal surface as strain proceeds. The net effect of strain localization is to reduce the rate of fresh area production on the plane normal to shear bands (the broad section, labeled B) at a constant crosshead speed. Since only the broad section is illuminated by the laser, this reduces the slope of the PSE versus strain plots in Fig. 5.

Stress and strain measurements provide little direct information about the progress of strain localization during tensile testing. The Considère criterion, for instance, provides only an upper bound on the strain at the onset of localization. Microstructure changes before the onset of global, mechanical instability are expected to reduce the strain at the onset of localization to values below that given by the Considère criterion—consistent with our interpretation of the PSE data in Table II. The lower values provided by the PSE data would be directly comparable to the predictions of models that incorporate the effect of microstructure on the onset of strain localization.

TABLE II. Strains given by the Considère criterion and the PSE signal slope discontinuity.

Alloy	Considère criterion	PSE discontinuity
1200	0.35±0.02	0.22±0.01
3003	0.26±0.02	0.20±0.01
5052	0.22±0.02	0.15±0.01
6061	0.23±0.02	0.20±0.01

V. CONCLUSIONS

Time-resolved laser-stimulated electron signals from 1200, 3003, 5052, and 6061 aluminum show a peak in the time-of-flight spectra (Peak I) that can be attributed to electrons passing directly from the metal surface without losing kinetic energy to inelastic scattering events. It is therefore sensitive to the production of fresh aluminum due to plastic strain. When the intensity of this peak is extracted from the data and plotted against the strain, the resulting graph shows a discontinuity in slope that we associate with the onset of

strain localization. In each case, this discontinuity occurs at strains somewhat below the onset of the mechanical instability predicted by the Considère criterion. This is consistent with the expectation that the Considère criterion provides an upper bound on the onset of strain localization in each case. The wide range of mechanical properties displayed by these alloys suggests that this technique may be broadly applicable. We expect that PSE measurements will provide reliable data for comparing constitutive models that predict the onset and course of strain localization—especially for models that make quantitative predictions of surface area production on each surface of the gauge section as a function of strain.

ACKNOWLEDGMENTS

This work was supported by the Department of Energy under Grant No. DE-FG03-02ER45988. The authors thank Chase Bradford, Washington State University, for assistance with the electron trajectory simulations.

[1]A. G. Considère, Ann. Ponts Chaussees 9, 574 (1885).
[2]E. W. Hart, Acta Metall. **15**, 351 (1967).
[3]M. J. Hillier, Int. J. Mech. Sci. **7**, 531 (1965).
[4]E. Duncombe, Int. J. Mech. Sci. **14**, 325 (1972).
[5]E. Duncombe, Int. J. Solids Struct. **10**, 1445 (1974).
[6]F. A. Nichols, Acta Metall. **28**, 663 (1980).
[7]F. Chemelík, A. Ziegenbein, H. Neuhäuser, and P. Luká, Mater. Sci. Eng., A **324**, 200 (2002).
[8]J. J. Jonas, R. A. Holt, and C. E. Coleman, Acta Metall. **24**, 911 (1976).
[9]A. K. Ghosh, Acta Metall. **28**, 1443 (1980).
[10]D. Peirce, R. J. Asaro, and A. Needleman, Acta Metall. **30**, 1087 (1982).
[11]D. Peirce, R. J. Asaro, and A. Needleman, Acta Metall. **31**, 1951 (1983).
[12]A. Korbel and P. Martin, Acta Metall. **36**, 2575 (1988).
[13]E. Estrin, C. P. Ling, and P. G. McCormick, Acta Metall. Mater. **39**, 2943 (1991).
[14]Y. Bréchet, G. Canova, and L. P. Kubin, Acta Mater. **44**, 4261 (1996).
[15]J. H. Giovanola, Mech. Mater. **7**, 59 (1988).
[16]J. W. Hutchinson, Scr. Metall. **18**, 421 (1984).
[17]W. J. Baxter and S. R. Rouze, J. Appl. Phys. **44**, 4400 (1973).
[18]J. T. Dickinson, L. C. Jensen, and S. C. Langford, J. Mater. Res. **9**, 1156 (1994).
[19]R. Holm, Vak.-Tech. **7**, 208 (1974).
[20]R. Holm and S. Storp, J. Electron Spectrosc. Relat. Phenom. **8**, 139 (1976).
[21]B. R. Strohmeier, Surf. Interface Anal. **15**, 51 (1990).
[22]I. Olefjord, H. J. Mathieu, and P. Marcus, Surf. Interface Anal. **15**, 681 (1990).
[23]L. P. H. Jeurgens, W. G. Sloof, F. D. Tichelaar, C. G. Borsboom, and E. J. Mittemeijer, Appl. Surf. Sci. **144–145**, 11 (1999).
[24]J. I. Eldridge, R. J. Hussey, D. F. Mitchell, and M. J. Graham, Oxid. Met. **30**, 301 (1988).
[25]L. P. H. Jeurgens, W. G. Sloof, F. D. Tichelaar, and E. J. Mittemeijer, Thin Solid Films **418**, 89 (2002).
[26]Y. Aoki, H. Fujii, and K. Nogi, J. Mater. Sci. **39**, 1779 (2004).
[27]K. Binns and P. Lawrenson, *Analysis and Computation of Electric and Magnetic Fields Problems*, 2nd ed. (Pergamon, New York, 1973).
[28]L. Grunberg, Wear **1**, 142 (1957).
[29]A. H. Meleka and W. Barr, Nature (London) **187**, 232 (1960).
[30]V. S. Kortov and R. I. Mints, Soviet Mater. Sci. 2, 197 (1966).
[31]J. A. Ramsey, J. Appl. Phys. **37**, 452 (1966).
[32]D. R. Arnott and J. A. Ramsey, Surf. Sci. **28**, 1 (1971).
[33]W. J. Baxter, Vacuum **22**, 571 (1972).
[34]W. J. Baxter, J. Appl. Phys. **44**, 608 (1973).
[35]W. J. Baxter, J. Appl. Phys. **45**, 4692 (1974).
[36]W. J. Baxter and S. R. Rouze, J. Appl. Phys. **46**, 2429 (1975).
[37]W. J. Baxter, Metall. Trans. A **6A**, 749 (1975).
[38]O. Buck, W. J. Pardee, F. J. Szalkowski, and D. O. Thompson, Appl. Phys. **12**, 301 (1977).
[39]J. T. Dickinson, P. Braunlich, L. Larson, and A. Marceau, Appl. Surf. Sci. **1**, 515 (1978).
[40]T. K. G. Swami and Y. W. Chung, Surf. Sci. **99**, 373 (1980).
[41]W. J. Baxter and S. R. Rouze, Rev. Sci. Instrum. **44**, 1628 (1973).
[42]G. I. Taylor, J. Inst. Met. **62**, 307 (1938).
[43]F. J. Humphreys and M. Hatherly, *Recrystallization and Related Annealing Phenomena* (Pergamon, New York, 1995).